Optimization of an eco-friendly hydraulic road binders comprising clayey dam sediments and ground granulated blast-furnace slag

Selma Bellara, Mustapha Hidjeb, Walid Maherzi, Salim Mezazigh, Ahmed Senouci

buildings

MDPI

Article

Optimization of an Eco-Friendly Hydraulic Road Binders Comprising Clayey Dam Sediments and Ground Granulated Blast-Furnace Slag

Selma Bellara [1,2,3,*], Mustapha Hidjeb [1], Walid Maherzi [2,*], Salim Mezazigh [3] and Ahmed Senouci [4,*]

1 Materials, Geotechnics, Housing and Urban Planning Laboratory (LMGHU), Faculty of Technology, University of 20 aout 1955-Skikda, 26 Route d'El-Hadaiek, Skikda 21000, Algeria; mustapha_hidjeb@yahoo.fr
2 University Lille, IMT Lille Douai, University Artois, JUNIA, ULR 4515—LGCgE, Laboratory of Civil Engineering and Geo-Environment, F-59000 Lille, France
3 Continental and Coastal Morphodynamics Laboratory (M2C), UMR 6143 CNRS, University Caen Normandie, 24 Rue des Tilleuls, F-14000 Caen, France; salim.mezazigh@unicaen.fr
4 Department of Construction Management, College of Technology Building, 4730 Calhoun Road #300, Houston, TX 77204-4020, USA
* Correspondence: selma.bellara@imt-lille-douai.fr (S.B.); walid.maherzi@imt-lille-douai.fr (W.M.); asenouci@uh.edu (A.S.)

Abstract: This study investigated the potential use of Zerdezas dam Calcined Sediments (CS) and El-Hadjar Blast Furnace Slag (GGBS) from northern Algeria as a partial replacement of cement (C) in normal hardening hydraulic road binders. Two binder mix designs were optimized using a Response Surface Methodology (RSM). The first mix, 50C35GGBS15CS, consisted of 50% cement, 35% blast furnace slag, and 15% calcined sediment. The second mix, 80C10GGBS10CS, consisted of 80% cement, 10% blast furnace slag, and 10% calcined sediments. The tests of workability, setting time, volume expansion, compressive and flexural strengths, porosity, and SEM were conducted to ensure that both mixes meet the standard requirements for road construction binders. The two proposed mixes were qualified as normal hardening hydraulic road binder. The reuse of the sediments will contribute to a better disposal of dam sediments and steel industry waste and to preserve natural resources that are used for manufacturing cement. It will also contribute to the environmental impact reduction of cement clinker production by reducing greenhouse gas emissions.

Keywords: hydraulic road binder; eco-friendly; calcined sediments; cement; granulated blast furnace slag

Citation: Bellara, S.; Hidjeb, M.; Maherzi, W.; Mezazigh, S.; Senouci, A. Optimization of an Eco-Friendly Hydraulic Road Binders Comprising Clayey Dam Sediments and Ground Granulated Blast-Furnace Slag. *Buildings* **2021**, *11*, 443. https://doi.org/10.3390/buildings11100443

Academic Editor: Jian-Guo Dai

Received: 27 August 2021
Accepted: 24 September 2021
Published: 28 September 2021

1. Introduction

Cement is the second most consumed material worldwide after water [1]. It is used in buildings, soil stabilizations, dams, bridges, roads, rails, and many other construction fields. Cement is considered as the most produced material by weight [1]. The global population growth in the last few decades has led to a rise in construction activities which has increased the demand for construction materials, and in particular, cement. The local cement production in Algeria amounts to 18 million tons with a gap amount of 5 million tons to cover the growing market demand [2]. A global production of 7 billion tons of cement or even more is expected in 2050 [3]. The need to keep up with the rising demand, particularly for developing countries, should be coupled with the necessity to better manage carbon dioxide emissions to reduce environmental impacts. Cement production is responsible for the emission of one ton of CO_2 for each ton of produced clinker [4–6]. It generates a global greenhouse gas emission amount of 5 to 8% of the entire CO_2 emissions [6,7]. This is due to its high energy process (i.e., clinkerization process at 1450 °C), which produces an equivalent energy of about 3.5 GJ per 1 ton of Portland cement clinker [8,9]. Two thirds of these emissions are due to the calcination of limestone

($CaCO_3$) and decomposition to calcium oxide (CaO), while the remaining third of these emissions are attributed to fossil fuel combustion [7,9,10]. Therefore, this has become a major environmental, industrial, and societal concern.

Several solutions were suggested to address sustainable development and combat global warming. In 2009, the International Energy Agency proposed carbon capture and sequestration to reduce the level of CO_2 emitted from cement production by 56% in 2050 [1,11]. This technology has not yet been proven and its application is still limited industrially [12]. Moreover, it is still relatively very expensive [1,13].

The most suitable and economical solution remains the replacement of cement by mineral additions [14]. This solution also preserves the supply of natural resources that are becoming scarce [8]. The partial replacement of cement with natural materials (pozzolan, limestone filler, metakaolin) or industrial byproducts, such as blast furnace slags, fly ash, and silica fume, have been extensively studied by researchers [3,13,15–17]. Moreover, greenhouse gas emissions can be reduced by the replacement of cement by GGBS and durability [17]. These studies have focused on investigating the performance of medium- and long-term pozzolanic potentials (excluding limestone filler) as well as low energy consumption. The energy needed for the calcination of kaolin during the manufacture of metakaolin is ten times lower than that for the manufacture of clinker [8]. However, the low availability of these natural materials and industrial byproducts calls for the adoption of new alternative materials as cement replacements. For example, fly ash represents only 30% of the total needed quantity. However, because of its varying quality, only one third or less of the available fly ash is currently used as mineral addition [14]. These quantities will further decrease in the coming years according to a study by the International Energy Agency on the achievement of the objective of limiting global warming to 2 °C in 2100 [9].

On the other hand, huge quantities of sediments settle every year in the bottom of dams. This situation causes a reduction of the water storage capacity for these dams. Regular dredging operations are therefore essential to extend the life of these dams. However, these dredging operations generate significant volumes of sediments, the management of which has become a major scientific and environmental issues over the past few decades. The Zardezas dam lost three quarters of its initial capacity with a siltation rate of 0.4 million m^3/year between 2003 and 2006. Thus, the Zardezas dam presents a short-term sedimentation risk [18]. The substitution of the cement matrix with kaolinite-containing clays has always been favored because of their high availability worldwide, especially in countries with high cement demand [1,9]. Moreover, recent studies have shown that clinker replacement with calcined sediments has been successful. Laoufi et al. (2016) [2] confirmed the high pozzolanic character of thermally treated Fergoug dam sediments at various temperature levels (750 °C, 850 °C, and 950 °C). Benzerzour et al. (2017 and 2018) [4,19] studied the mechanical properties of a mortar in which the cement was replaced by 750 °C calcined marine French sediments. They reported that the mechanical properties of the mortar were equal to or higher than those of the control mortar. Similarly, Dang et al. (2013), Hadj Sadok et al. (2021), Snellings et al. (2016), and van Bunderen et al. (2019 and 2021) [20–24] highlighted the effect of using calcined sediment as a supplementary material on the mechanical properties of mortars and concretes.

Few studies have been carried out on adding supplementary cementitious material to prepare hydraulic road binders. Stevulova et al. (2021) [25] studied the incorporation of granulated blast furnace slag, ground limestone, and cement bypass dust to produce a normal hardening hydraulic road binder. Segui et al. (2013) [5] evaluated the effect of natural pozzolan on the stabilization of a clayey soil as a main component of the produced hydraulic road binder.

This paper presents an experimental study to optimize ternary eco-friendly hydraulic road binders based on El-Hadjar blast furnace slag and calcined sediments from the Zardezas dam in Skikda city in northern Algeria. The assessment of the microstructure development of the blended binders by mercury intrusion porosimetry (MIP) and thermogravimetric analysis (TGA), in comparison to OPC blended cement, was carried out.

The chemical and mechanical performance of mixtures were also evaluated and quantified by compressive (UCS), flexural strength (ITS), and leaching tests. The characterizations of the fresh states of the mixtures were carried out by measuring the soundness and the setting time. The study also aims to assess the potential of reusing waste and byproducts as supplementary material for the production of hydraulic road binders according to the specifications.

2. Materials and Methods

2.1. Cement

The cement used was a CEM I 42.5 N composed of 95% to 100% of clinker and 0 to 5% of secondary components. It had an initial setting time higher than 60 min and an expansion lower than 10 mm in accordance with NF EN 197-1. The cement had an unconfined compressive strength between 42.5 MPa and 62.5 MPa on day 28. Table 1 summarizes the cement physical and chemical properties. Figure 1 shows the cement grain size distribution.

Table 1. CEM I 42.5 N physical and chemical properties.

Physical Properties	Values	Major Oxides	Percentage (%)
SSA BET (cm^2/g)	9194	SiO_2	17.13
Density (g/cm^3)	3.16	Al_2O_3	4.51
D10	1.09	FeO_3	2.95
D50	12.09	CaO	60.13
D90	43.50	MgO	0.78
		SO_3	4.09
		K_2O	1.01
		Na_2O	0.29
		TiO_2	0.32
		MnO	Traces
		BaO	Traces
		SrO	Traces
		OF2	—

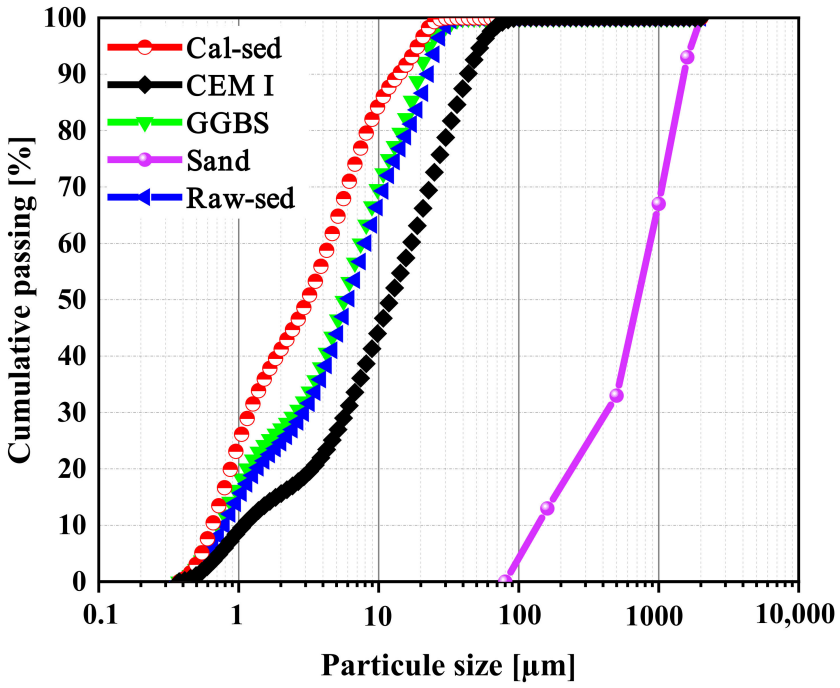

Figure 1. Particle size distribution of cement, GGBS, sand, and other supplementary materials.

2.2. Ground Granulated Blast Furnace GGBS

The slag used was collected from El-Hadjar steel plant in the city of Annaba in northeastern Algeria. The steel production in this complex generates 500,000 tons per year. About 60% of the steel is cooled quickly right out of the blast furnace and is let to solidify and form vitreous material with grain sizes ranging from 0 to 5 mm [26]

The granulated slag was subsequently finely grinded in the laboratory using the RS 200 vibratory Disc Mill by Retsch. Table 2 summarizes the slag physical and chemical properties. Figure 1 shows the GGBS grain size distribution.

Table 2. GCBS physical properties and major oxide content.

Physical Properties	Values	Major Oxides	Percentage (%)
SSA BET (cm^2/g)	9171	SiO_2	34.35
Density (g/cm^3)	2.95	Al_2O_3	7.83
D10	0.73	FeO_3	0.76
D50	5.70	CaO	41.47
D90	20.09	MgO	4.09
		SO_3	1.56
		K_2O	1.19
		Na_2O	0.26
		TiO_2	0.27
		MnO	1.48
		BaO	1.56
		SrO	0.24
		OF2	0.82

2.3. Sand

The standard siliceous sand, which was used for preparing the mortars, had a silica content of 98% and a maximum diameter of 2 mm (Standard CEN 196-1 ISO). The sand grain size distribution is shown in Figure 1.

2.4. Raw Sediment Origin and Sampling

The sediments used in this study come from the Zardezas dam in the wilaya of Skikda in northeastern Algeria; its location is shown in Figure 2. A random sampling was taken upstream of the dam using a hand shovel at a depth between 0 and 70 cm.

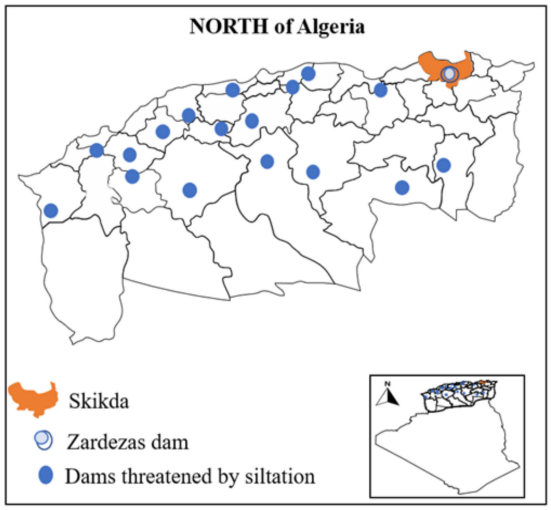

Figure 2. Zardezas dam location [27].

The sediments were transported to the laboratory in plastic bags. They were first air dried and then heated in an oven at 50 °C to avoid any modification or alteration of

their chemical composition. The sediments were then crushed and homogenized. The initial water content, which was measured according to standard NF P94-050, was valued between 47% and 53%. The particle size distribution of the sediments was carried out using the dry method on an LS 13320 laser diffraction (particle size analyzer, Beckmann Coulter company, Brea, CA, USA). Figure 1 shows that the sediments were mainly composed of fine fractions with a D50 of 6.15 µm and a D90 of 22.43 µm. The moisture content, which was determined by loss on ignition at 550 °C in accordance with the standard NF EN 15169, was equal to 6.29%. The absolute density of the sediments was determined according to NF EN 1097-7 using Micromeritics AccuPyc 1330 helium pycnometer. On the other hand, the Micromeritics Autopore IV 9505 was used for the determination of the specific surface area BET according to NF EN ISO 18757.

The geotechnical characteristics were also determined to provide information on clay fraction. The methylene blue value and Atterberg limits were determined according to NF P94-068 and NF P94-051, respectively.

2.5. Optimization of the Thermal Activation/Treatment of Sediment

Characterization of Calcined Sediment

A thermal gravimetric analysis was used to determine the optimal calcination temperature. A QMS 403D-NETZSCH instrument with Argon flow rate of 60 mL/min was used for this purpose, with a heating rate of 2 °C/min from 35 °C to 40 °C and 3 °C/min from 40 °C to 1000 °C. The temperature during the first phase of decomposition ranged from 40 °C to 225 °C. The mass loss during that phase, which is shown in Figure 3, was probably attributed to the evaporation of surface and interlayer adsorbed water [28,29]. A small mass loss in the range of 225 °C to 320 °C was probably due to the decomposition of ferric oxyhydroxide [28].

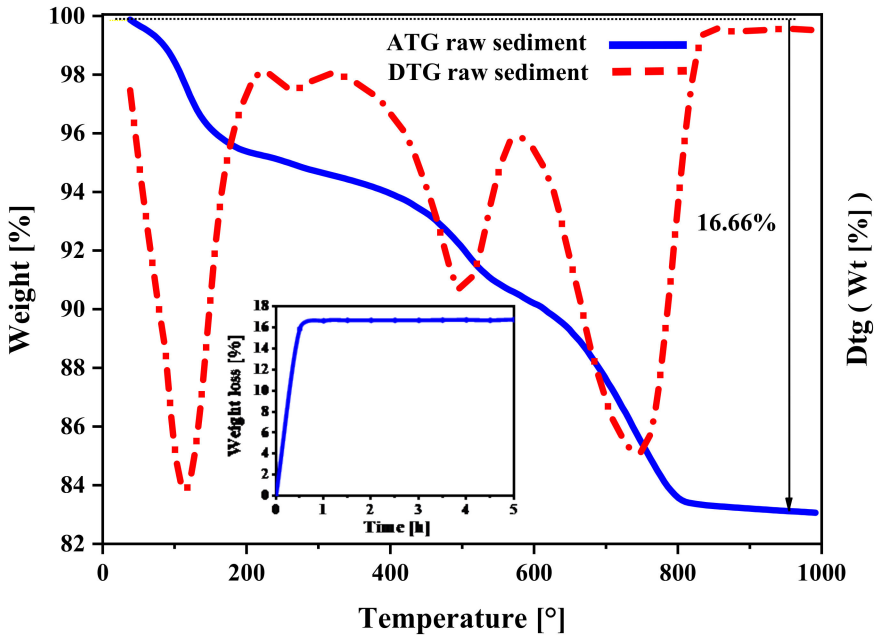

Figure 3. Sediment weight loss variation with time and temperature.

A mass loss of organic matter occurred between the temperatures of 450 °C and 550 °C [29]. The dihydroxylation of the various minerals in Zardezas sediments occurred between the temperatures of 350 °C to 800 °C. On the other hand, the decomposition of calcite $CaCO_3$ (decarbonation) also took place between the temperatures of 550 °C to 800 °C [30].

The calcination time was determined as follows. The samples were heated in an oven at a temperature of 800 °C and their mass stability was monitored for a duration of 5 h.

Figure 3 shows that the mass loss became very negligeable (almost equal to zero) after 1 h of thermal treatment, which indicates that the various decomposition stages (loss of organic matter, dihydroxylation of clay minerals, and decarbonation of $CaCO_3$) were been completed [4,31] Therefore, the calcination was set for a duration of 1 h at a temperature of 800 °C [4] to ensure an optimal pozzolanic reactivity and to avoid the risk of recrystallization.

The thermal treatment allowed the creation of an amorphous disordered structure for the material, which conferred a pozzolanic characteristic to the sediments. This led to the formation of calcium silicate and calcium aluminate hydrates when the treated sediments reacted with cement portlandite, at a normal temperature and in an alkaline medium (Standard EN 197-1).

Figure 4 presents a visual aspect of raw dried, calcined, and crushed calcined sediments. It shows that the sediments took on a reddish color after calcination, due to the presence of iron in the sediments. The change in color appeared even at a low iron content [14].

(**a**) (**b**) (**c**)

Figure 4. Visual aspect of (**a**) raw dried; (**b**) calcined and (**c**) crushed calcined sediment.

2.6. Chemical and Mineralogical Composition of Raw Sediment and Supplementary Material

The chemical compositions of the materials used in the study, which are summarized in Tables 1–3, were determined using S4 PIONEER X-ray fluorescence (XRD) spectrometer by BRUKER. Figure 5 shows XRD diffraction patterns of GGBS and sediments. The main oxides present in the Zardezas sediments were silicon (SiO_2), Aluminium (Al_2O_3), and calcium (CaO) along with small percentages of MgO, K_2O, Na_2O, and TiO_2. The percentage of SiO_2, Al_2O_3 and Fe_2O_3 in the calcined sediments was equal to 77.99%, which is higher than the threshold of 70% set by ASTM C168-03 for pozzolanic materials. The low amount of sulfate (SO_3) in the treated sediment may have resulted from the decomposition of an organic matter [4].

The crystal structures of the GGBS and the sediments were determined using a BRUKER D8 Focus diffractometer, which is an X-ray source employing Cukα radiation with a wavelength of λkα = 1.74 Å. A 2θ angle range between 5 and 80° was used along with a step size of about 0.02° and a time step size of one second. A current of 30 mA and a voltage of 40 kV were also used.

The Zardezas sediment is composed of three main phases, namely, silicates (Quartz (SiO)), carbonate (calcite ($CaCO_3$) and dolomite), and clay minerals (Kaolinite, Albite, Chlorite, and Illite).

Alujas et al. (2015) and Avet et al. (2016) [28,32] have shown that the reactivity of a clay depends largely on the amount of kaolinite it contains. The compressive strength of an LC3 mortar with 40% kaolinite, which contained 50% clinker, 30% calcined clay, 15% limestone filler (15%), and 5% gypsum, reached Portland cement strength after 7 days of curing. The presence of kaolinite in the Zardezas dam sediments is a good indication of their pozzolanic potential.

Table 3. Physical and chemical characteristics of raw and treated sediments.

Physicochemical Properties	Raw Sediment	Calcined Sediment
Water content (%)	49.86	0
Clayey fraction Dmax < 2 µm	23.6	39.57
Silty fraction 2 µm < Dmax < 63 µm (%)	76.4	60.43
Density (cm^2/g)	2.63	2.75
Plasticity index (%)	29.9	—
Blue methylene value (g/100 g)	4.41	—
$CaCO_3$ (%)	15.55	—
SiO_2	48.27	51.84
Al_2O_3	17.73	19.23
FeO_3	6.26	6.92
CaO	9.35	10.2
MgO	2.11	2.41
SO_3	—	0.28
K_2O	2.25	2.47
Na_2O	0.36	0.38
TiO_2	0.81	0.9

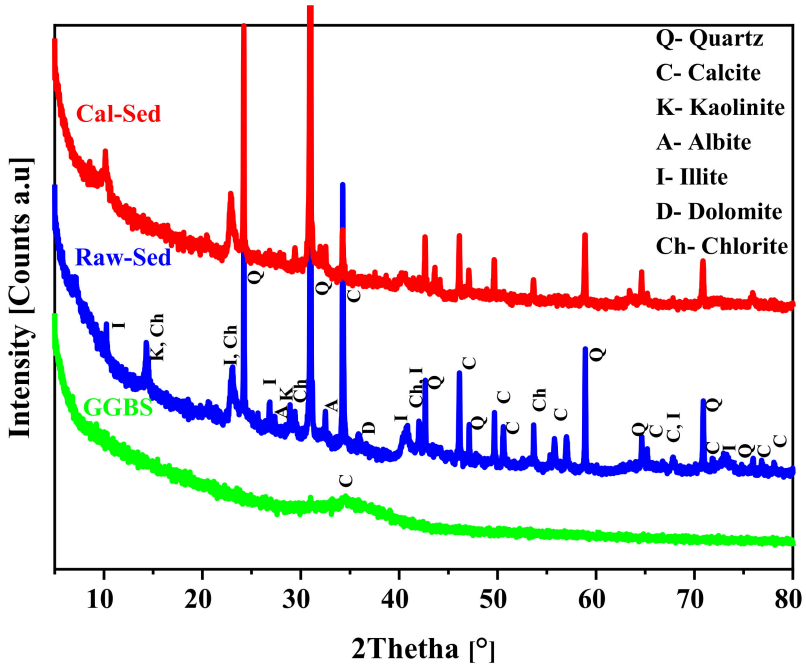

Figure 5. XRD diffraction patterns of GGBS and sediments.

The XRD patterns of the calcined sediments showed that Kaolinite completely disappeared after heating, due to the dehydroxilation and the kaolinite transformation into metakaolin at a temperature between 650° and 850° [2]

2.7. Leaching Tests

Water leaching tests were performed on raw sediments in compliance with NF EN 12457-2 to evaluate their pollution levels. Table 4 summarizes the water leaching test results. A chemical analysis was also conducted using the inductively coupled plasma optical emission spectroscopy (ICP-OES 5100 Agilent Technologies). The test was kept under agitation for 24 h to allow for the extraction of sediment heavy metals. In the test, a liquid to solid ratio of 10 L/kg was used while the element concentrations were all below the inert waste reference values in accordance with the French Directive of 14 December 2014. The Zardezas sediment can be qualified as inert and suitable for valorization without treatment.

Table 4. Water leaching test results for raw sediments and inert wastes.

Elements	Raw Sediment	Inert Waste Reference
	(mg/kg of Dry Matter)	(mg/kg of Dry Matter)
As	<0.11	0.5
Ba	0.57	20
Cd	<0.009	0.04
Cr	<0.004	0.5
Cu	0.064	2
Mo	<0.088	0.5
Ni	<0.047	0.4
Pb	<0.023	0.5
Sb	<0.057	0.06
Se	<0.083	0.1
Zn	0.02	4
Chloride	39.5	800
Fluoride	7.15	10
Sulfate	515	1000
Soluble fraction	1000	4000.00

2.8. Mix Design

The Design of Experiments (DOE) consists of evaluating simultaneously the effects of factors (i.e., inputs variables) on the system responses (i.e., outputs variables) using a surface response method [33]. DOE yields substantial savings in time and cost because it allows for gathering a maximum amount of information for a limited number of experiments. Fatemi et al. (2006) [34] used factorial and fractional factorial designs to optimize a sustainable road market paint. X. Li et al. (2012) [35] used a central composite design to evaluate the combined effects of MgO, SO_3, temperature, and sintering time during clinker sintering. Imanzadeh et al. (2018) [36] studied the influence of silt, lime, cement, and water in a D-optimal mixture design on the unconfined compressive strength of raw earth concrete. Other researchers have also shown an interest in the use of DOE in the civil engineering field [33,37,38].

An optimal mixture was designed herein for the optimization of a hydraulic road binder using a statistical and mathematical computer-generated design for irregular experimental regions [36]. The software evaluated the effect of cement (C) (i.e., variable X1), granulated ground furnace slag (GGBS) (i.e., variable X2), and calcined sediment (CS) (i.e., variable X3) on the mortar unconfined compressive strength at 28 days of age. Equation (1) limits the sum of components to a value of one (100%). Moreover, the optimal mixture design method specifies low and high limits for each factor (i.e., mixture component). These limits must be between the values of 0 and 1 (0–100%), as summarized in Table 5.

$$\sum_{i=1}^{i=n} Xi = 1, \text{ with } 0 < Xi < 1 \quad (1)$$

Table 5. Mixture component value limits.

Value Limits	X_1 (C)	Variables X_2 (GGBS)	X_3 (CS)
Low	50	0	0
High	100	50	30

Figure 6 shows the experimental design space, which was built by applying a quadratic polynomial model using Design Expert software. The red points represent the 11 mixtures to be tested.

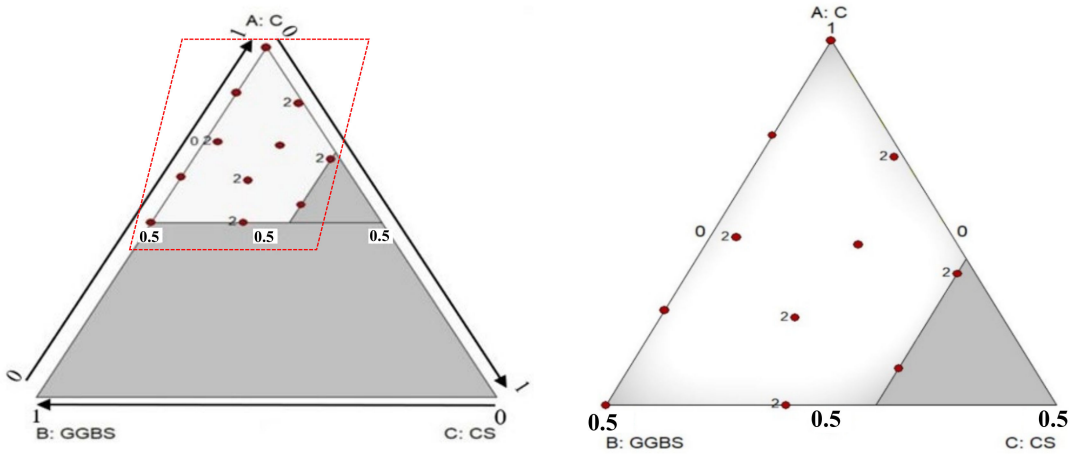

(**a**) (**b**)

Figure 6. (**a**) Experimental design space; (**b**) experimental points distribution within the experimental design space.

2.9. Testing Protocol

2.9.1. Specimen Sizes

First, 4 × 4 × 16 cm mortar prisms were prepared according to NF EN 196-1. Table 6 summarizes the 11 mix designs. In this study, three mixes (two optimal formulations and a control) were considered. The first one, which is labelled as 50C35GGBS15CS, consisted of 50% cement, 35% blast furnace slag, and 15% calcined sediment. The second mix design, which is labelled 80C10GGBS10CS, consisted of 80% cement, 10% blast furnace slag, and 10% calcined sediments. Finally, the third mix is the control containing only cement (i.e., reference mortar). A water cement ratio (W/C) of 0.5 ratio was used in all mixes. The method of mixing, molding, and curing of the specimens followed NF EN 196-1.

Table 6. Mix designs.

Mix Designs	Cement (C)		G: Granulated Blast Furnace (GGBC)		CS: Calcined Sediment	
	(%)	(g)	(%)	(g)	(%)	(g)
84C01GGBS15CS	84	378	01	5	15	68
68C02GGBS30CS	68	306	02	09	30	135
72C11GGBS17CS	72	324	11	50	17	77
55C15GGBS30CS	55	248	15	68	30	135
73C24GGBS03CS	73	329	24	108	03	14
63C37GGBS00CS	63	284	37	167	00	00
100C00GGBS00CS	100	450	00	00	00	00
87C13GGBS00CS	87	392	13	59	00	00
50C30GGBS20CS	50	225	30	135	20	90
62C23GGBS15CS	62	279	23	104	15	68
50C50GGBS00CS	50	225	50	225	00	00

2.9.2. Fresh Mortar Consistency

The slump test was used to determine the mortar consistency on the flow table according to NF EN 1015-3 at 0 min, 30 min, 60 min and 90 min. All the mixes were kept in sealed plastic bags at 20 °C to preserve their moisture.

2.9.3. Setting Times

The Vicat apparatus was used for the determination of the initial and final setting times standard consistency cement paste that was prepared and mixed in accordance with NF EN 196-3. The initial setting time is declared when the needle reaches a distance of

6 mm ± 3 mm from the base plate of the Vicat apparatus. On the other hand, the final setting time is declared when the needle penetrates the cement paste for a depth of 0.5 mm.

2.9.4. Soundness

Le Chatelier apparatus was used to determine the volumetric expansion (swelling) with a standard consistency. According to NF EN 196-3 measurements are obtained after 24 h. Then, the sample pastes are left to boil in a thermostatic bath for 3 h.

2.9.5. Mechanical Strength

The compression and flexural strength (USC and Rf) were determined using 4 cm × 4 cm × 16 cm samples in accordance with NF EN 196-1after 7, 28, 56 and 90 days of curing in water at 20 °C. The strength results at each curing day correspond to the average of three values.

2.9.6. Mercury Intrusion Porosimetry (MIP)

The porosity affects the mechanical behavior and durability of hardened mortar due to the capability of pores to interact with the external environment [4]. The pore volume and pore size distribution for small mortar fragments after drying at 40 °C were measured at 7, 28, 60, and 90 days using a mercury porosimetry analysis technique on Micromeritics AutoPore V 9600 in accordance with ISO 15901-1:2016.

2.9.7. Portlandite Quantification

Thermogravimetric analysis was performed on 200 mg mixes after 7, 28, 60, and 90 curing days to quantify their calcium hydroxide content. The quantity of calcium hydroxide produced by cement corresponds to the amount of water released by portlandite during its decomposition phase (dehydration) multiplied by a ratio of $\frac{74}{18}$ according to the following Equation (2) [39]

$$\begin{array}{c} Ca(OH)_2 \Rightarrow CaO + H_2O \\ (74\ g/mol) \quad (56\ g/mol)\ (18\ g/mol) \end{array} \tag{2}$$

The amount of portlandite was calculated by the tangent method within the 400–550 °C range using the following Equation (3):

$$\%Ca(OH)2 = \frac{\Delta(Wt\ 400\ ^\circ C, Wt\ 550\ ^\circ C) \times 74}{18} \tag{3}$$

where 74 = Molar Mass of CH (portlandite), 18 = Molar Mass of H_2O; Δ(Wt 400 °C, Wt 550 °C) = mass loss between 400 °C and 550 °C.

2.9.8. Scanning Electron Microscopy (SEM)

Scanning electron microscopy (SEM) was conducted using a Hitachi S-4300SE/N equipped with a Thermo Scientific Ultradry EDX detector. A Backscatter Electron Image (BSE) was used on a finely polished section of 1 cm^3 samples, which were impregnated in Epofix resin by Struers. A vacuum impregnation apparatus by Struers Epovac was used to avoid any air bubbles before and after the resin coating for about 5 min. The samples were placed in the oven for at least 48 h at 40 °C to allow the resin to harden before the polishing step. The polishing was accomplished using Struers Tergamin 20 in two successive steps. The first one consisted of coarse polishing in the order of 80, 220, 500 and 1200 using the MD-piano diamond grinding disc and ethanol lubricant. The second step consisted of fine polishing with MD Dac with diamonds particles of 6, 4, and 1 µm and DP brown lubricant. The BSE mode on carbon-coated (a thin conductive layer) polished sample was used to visualize the repartition of hydration products of cement mortar by distinguishing shades of grey in a different light. A secondary electron image (SE) on a gold-coated (a thin conductive layer) polished sample was used to visualize particle morphology images at

an accelerating voltage of 15.0 Kv and 5.0 Kv, and 15 mm and 10 mm working distances. Figure 7 shows the CS and GGBS grain morphologies.

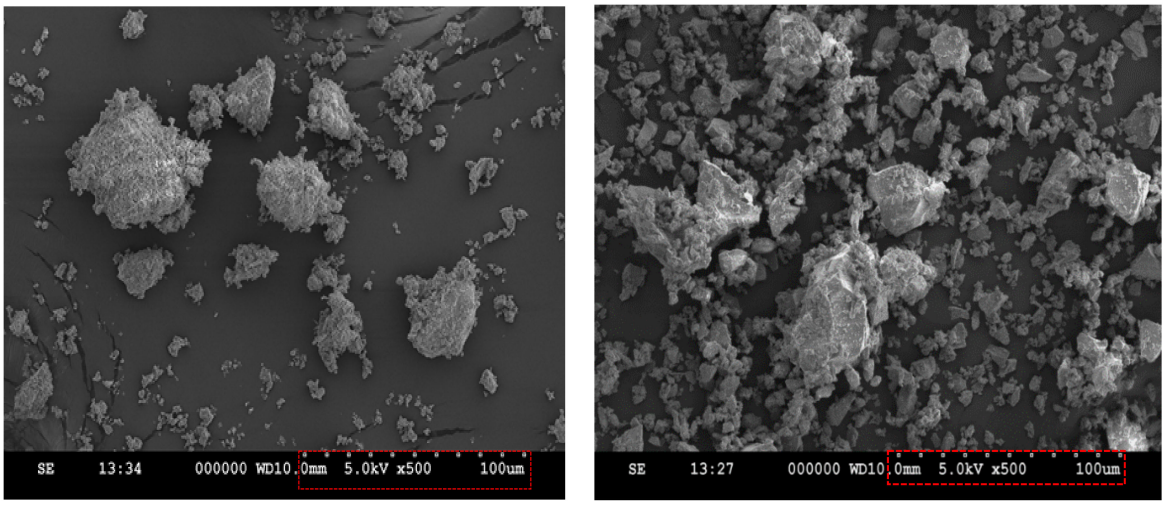

(**a**) (**b**)

Figure 7. (**a**) CS grain morphology; (**b**) GGBS grain morphology by secondary electron microscopy.

3. Results and Discussion

3.1. Validation of Predicted Models

The compressive strength for the 11 mix designs, which were obtained using Statease software, was determined at 28 days. The obtained strength results were modeled using the polynomial regression second degree of Scheffé, as suggested by the software.

The selection of the polynomial regression model was done according to the statistical analysis results. The quadratic model was selected instead of the special cubic model because it represents the most suitable model based of the values of *p*-value, adjusted R^2, and predicted R^2, conforming to guidelines. The *p*-value was statistically significant and lower than 0.05 while the adjusted and predicted R^2 were very close to 1 and their difference was lower than 0.2.

The 2D and 3D graphic surfaces shown in Figure 8 illustrate a surface response with different color shades from dark blue (i.e., lower resistances) to orange (i.e., higher resistance). Equations (4) and (5) are the selected regression models that relate the mix compressive strength to the three variables of cement, GGBS, and CS.

$$\text{USC } 28(\text{MPa}) = \text{C} \times \beta 1 + \text{GGBS} \times \beta 2 + \text{CS} \times \beta 3 + \text{C} \times \text{GGBS} \times \beta 12 + \text{C} \times \text{CS} \times \beta 13 + \text{GGBS} \times \text{C}\beta 23 \quad (4)$$

where,

$\beta 2$, $\beta 3$, $\beta 12$, $\beta 13$ and $\beta 23$ are the predicted model terms for the regression model.

$$\begin{aligned}\text{USC } 28(\text{MPa}) = \quad & \text{C} \times 41.73 + \text{GGBS} \times (-29.17) + \text{CS} \times (-105.83) + \text{C} \times \text{GGBS} \times 120.9 \\ & + \text{C} \times \text{CS} \times 165.16 + \text{GGBS} \times \text{C} \times 133.24\end{aligned} \quad (5)$$

To validate the selected regression model, the compressive strength of the two mixtures with new proportions was tested after 28 curing days. Table 7 shows that the compressive strength of the mixtures, which were determined experimentally, were well within the 95% confidence interval. This confirms the suitability of the selected model.

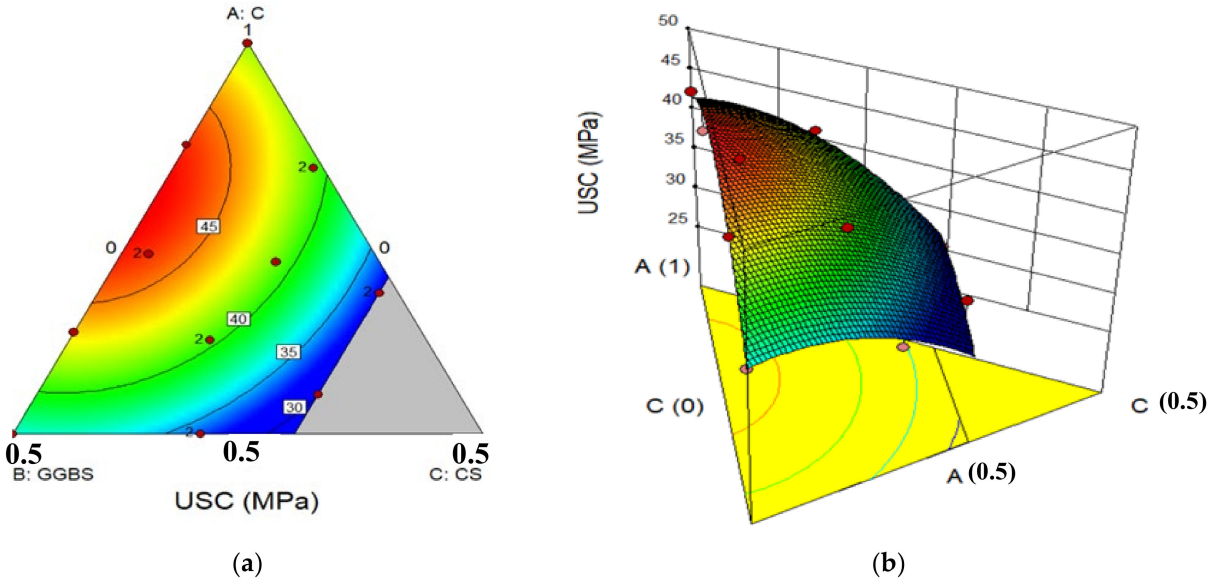

Figure 8. (**a**) 2D and (**b**) 3D response surfaces.

Table 7. Predicted and experimental USC after 28 days of curing.

Mix Design	Model Predicted USC (MPa)	95% CI (MPa)	Experimental USC (MPa)
50C35GGBS15CS	35.32	[33.37, 37.32]	35.17
80C10GGBS10CS	44.10	[42.69, 45.54]	45.18

3.2. Fresh Mortar Consistency

Figure 9 shows the variation mean flow diameter values as a function of time for the mixes 100C0GGBS0CS (control), 50C35GGBS15CS, and 80C10GGBS10CS. The initial flow value (at t = 0 min) for the mixes 100C0GGBS0CS, 50C35GGBS15CS, and 80C10GGBS10CS, which were measured according to EN 1015-3, were 227.5 mm, 216.5 mm, and 214.0 mm, respectively. The workability of the mixes 50C35GGBS15CS and 80C10GGBS10CS suffered a loss of 5% and 6%, respectively, compared to that of the control. Hence, they experienced almost the same workability loss, with a difference of about 1% (2 mm), Shanmuga Priya et al. (2020) [17] also highlighted a workability loss with cement replacement by GGBS of the order of 10%, 20%, and 30%. The workability loss can be attributed to the difference in the fineness of the used materials. In fact, the finer the material is, the higher its specific area and water demand. The workability of fresh mortar is controlled by several factors, such as fineness, water to binder ratio, shape of particles, and hydration rate [25,40]. Figure 7 shows an angular shape for SCM. Moreover, the bound water, which is released from the clay during the thermal treatment, could contribute to the increase of the demand for water [2].

The three mixes are qualified as plastic even after 90 min because their flow values are higher than the threshold limit of 140 mm [41]. The cement substitution by the supplementary materials can lead to a workability decrease as reported in previous studies [4,25]. However, the workability decrease remains negligible.

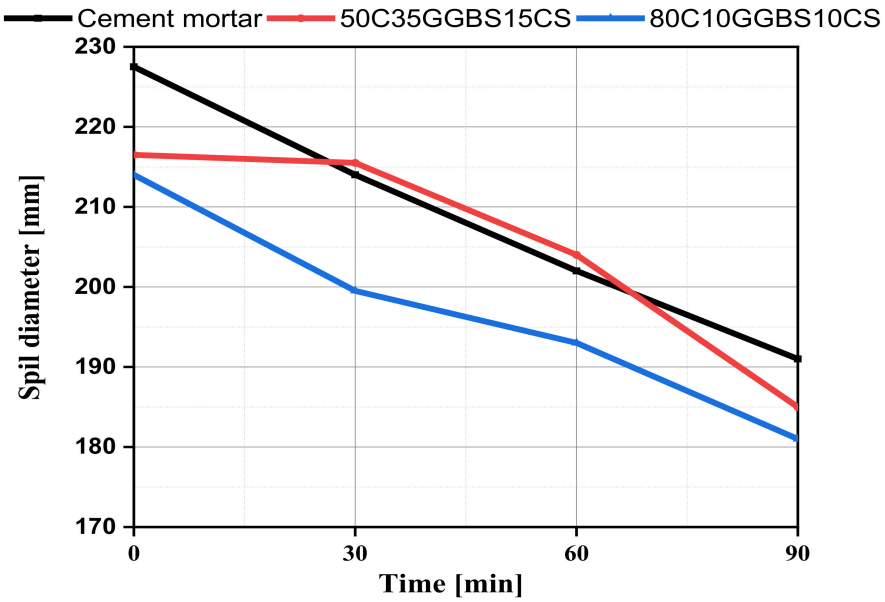

Figure 9. Evolution of flow value as a function of time.

3.3. Initial and Final Setting Times

The determination of the initial and final setting times is illustrated in Figure 10. The mixes 100C0GGBS0CS and 50C35GGBS15CS had an initial setting time of 250 min. The mix 80C10GGBS10CS had an initial setting time of 230 min. Therefore, the substitution of 20% of the cement by slag and calcined sediment caused an 8% decrease in the initial setting time compared to the reference mixture. The final setting time was 330 min for the mix 80C10GGBS10CS. However, it was equal to 360 min for the mixes 100C0GGBS0CS and 50C35GGBS15CS. Thus, the initial and final setting times decreased by substituting 20% of the cement with calcined sediments and GGBS. This can be explained as follows. Samet et al. (2007) [42] reported that the substitution of cement by calcined kaolinitic clay increases the hydrolysis rate of cement tricalcic silicates and calcined clay aluminates. Moreover, Wang et al. (2021) [43] reported that the setting time decrease of LC3 cements (limestone calcined clayed cements) is due to the large specific surface area (SSA) of calcined clay, which reduces the amount of free water in the matrices. The extend of initial and setting time by increasing the supplementary materials for 50C35GGBS15CS compared to 80C10GGBS10CS can be attributed to the pozzolanic reaction [43] On the other hand, a few of the heavy metals present in the sediments, such as zinc or nickel, can delay the setting time of the binders [19]. In this study, the setting times were not strongly influenced because the clayey sediments did not provide significant concentration of heavy metals. According to EN 13282-2, the obtained setting times are considered normal for road binders because they are greater than 150 min. These results are in accordance with those reported in previous studies [42,43].

3.4. Fineness and SO_3 Contents

The 90 µm mass residues were experimentally measured for the mixes using a grain size distribution analysis. Table 8 shows that the residue by mass at 90 µm percentages for different mixes were very low (close to zero). Increasing the mineral addition rates decreased the residue by mass at 90 µm in the hydraulic road binders. For example, the residue by mass at 90 µm reduction for the mixes 50C35GGBS15CS and 80C10GGBS 10CS were 50% and 20% than that of the control, respectively. These results agree with those reported by Stevulova et al. (2021) [25]. The mixes in this study satisfied the EN 13282-2 condition for normal hardening hydraulic road binder because their percentages of residue by mass at 90 µm were less than 15%.

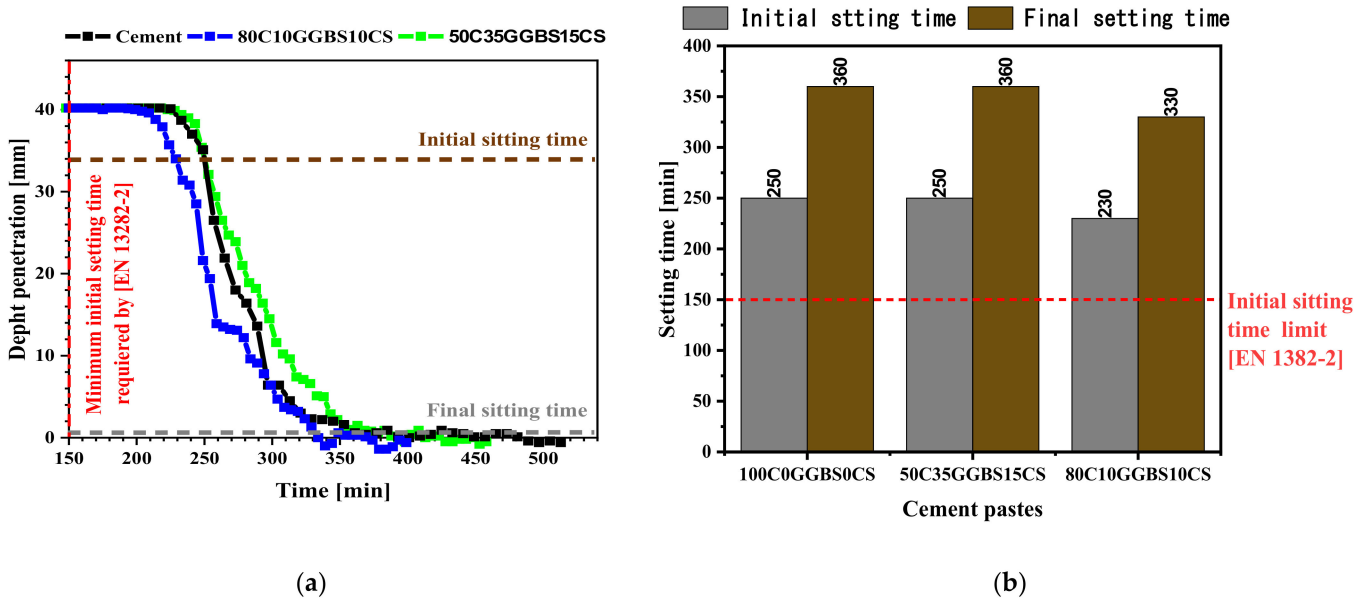

Figure 10. (**a**) Determination of setting time; (**b**) Initial and final setting time for various cement pastes.

Table 8. Binder residue by mass at 90 µm and sulfates contents.

	50C35GGBS15CS	80C10GGBS10CS	CEM I 42,5N	Threshold Limit Value [EN 13282-2]
Residue by mass at 90 µm (%)	0.18	0.28	0.35	15
Sulfate content (%)	2.63	3.46	4.09	4

Table 9 also summarizes the mixes sulfate mass concentrations, which were obtained using X-ray fluorescence analysis. The sulfate concentrations in the mixes 80C10GGBS10CS and 50C35GGBS15CS are equal to 2.63% and 3.46%, respectively. It is worth noting that these values are lower than that for the control mix, which is equal to 4.09%. Therefore, the sulfate contents for both mixes are well below the EN 13282-2 standard value of 4%, which is required for normal hardening hydraulic road binders. These results agree with those obtained by Stevulova et al. (2021) [25].

Table 9. Mixture expansion values.

Mixtures	100C0GGBS0CS	50C35GGBS15CS	80C10GGBS10CS
Volume expansion (mm)	0.330	1.280	0.740
Standard deviation (mm)	0.014	0.021	0.028

3.5. Binder Expansion

The mechanical properties of cementitious matrices can be affected by excessive volumetric instability/expansion, which can lead to material damage [44]. This volumetric instability is mainly induced by the chemical reactions of the cement hydration products ($Ca(OH_2)$, primary ettringite, etc.) with the chemical elements provided either by the aggregates and/or the external environment. More than 5% of MgO can affect the volume stability, leading to cracks in the cementitious matrices during the hardening period. Moreover, the free lime (CaO) content can cause a volume change when it hydrates.

Table 9 and Figure 11 summarize the volume expansion values for all binder mixes. The replacement of cement by ground granulated blast furnace and calcined clayey sediments increased the volume expansion value. The volume expansion of the mix 80C10GGBS10CS mixture (0.74 mm) was more than double that of the control (0.33 mm).

Moreover, the volumetric expansion of the mix 50C35GGBS15CS was 1.28 mm, which is more than four times that of the control. This can be because the MgO content in GGBS (4.09%) and in CS (2.41%) was higher than that in the cement (0.78%). This can also be due to the probable formation of Brucite ($Mg(OH)_2$), generated by the hydration of MgO (periclase) and the free lime content. However, the increased volume expansion remains very low and not significant when compared to the threshold limit value of 30 mm for normal hardening hydraulic road binders (EN 13282-2).

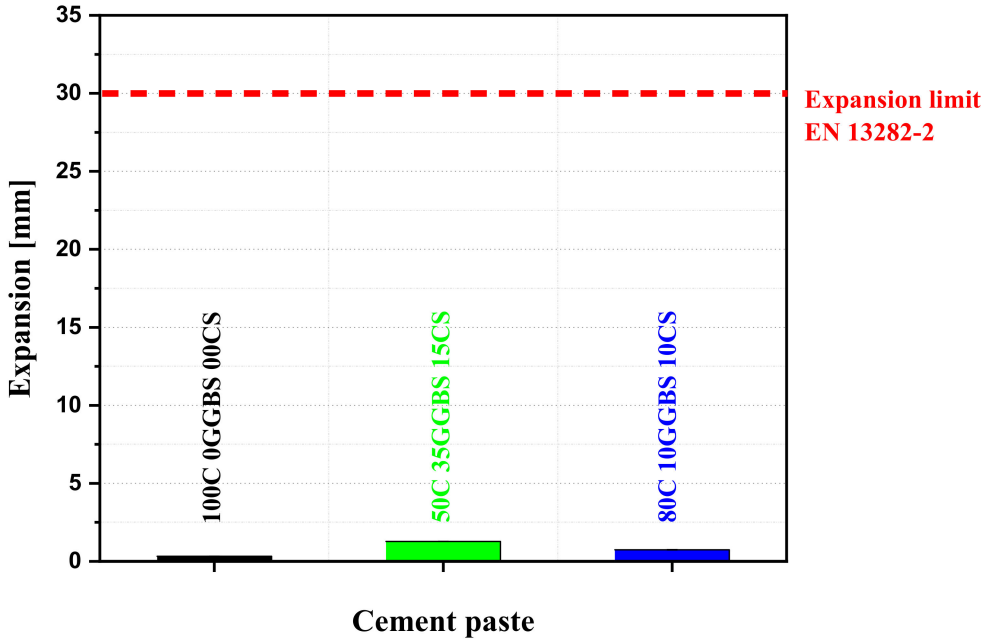

Figure 11. Cement paste expansion values.

3.6. Compressive and Flexural Strengths

Figure 12 summarizes the compressive and flexural strength values over time for the three mixes. After 28 days of curing, the compressive strengths of the mixes 50C35GGBS15CS and 80C10GGBS10CS were 28.82% and 8.56% lower than that of the control. This strength loss tends to decrease with curing time. In the long term, the mixes 50C35GGBS15CS yielded a higher compressive strength than that of control one.

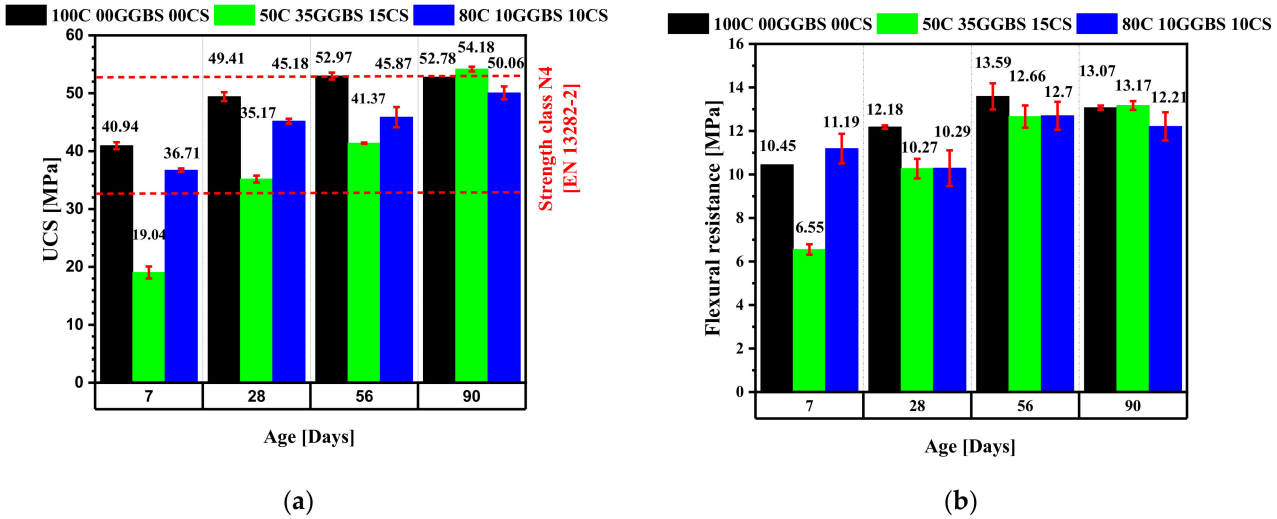

Figure 12. Mix (**a**) compressive and (**b**) flexural strengths at 7, 28, 56, and 90 curing days.

The significant strength increases for the mixes with GGBS and CS, which occurred between 7 and 90 days of curing, were due to pozzolanic reactions. The reaction of portlandite ($Ca(OH)_2$), which is a cement and GGBS hydration product, with the reactive aluminosilicates phases of slag and calcined clayey sediments, formed more C-S-H gel (see Equations (6) and (7)). Thereby, the formation of the new CSH gel reduced the porosity of the cementitious matrices, which in turn improved the mechanical performance of the mixes. Several previous studies have reported on the effective role of pozzolanic reactions in enhancing the compression strength and durability of cementitious mortars [2,4,6,19,29]

$$3\,CH + 2\,S \rightarrow C_3S_2H_3 \quad (6)$$

$$A + F + 8\,CH + 18\,H \rightarrow C_8AFH_{26} \quad (7)$$

where CH = Portlandite, S = SiO_2, A = Al_2O_3, F = Fe_2O_3, and H = H_2O.

The two road binders fall into the class of normal hardening hydraulic road binder (class N4 binders) according to EN 13282-2, which states that the UCS after 56 days of curing is between 32.5 MPa and 52.5 MPa. All the mixes yielded sufficient strength values, meeting the mechanical strength requirements for road construction after 56 days of curing. These results agreed with those reported by Stevulova et al. (2021) [25].

The flexural strength of the mixes also increased with curing time. After 28 curing days, the flexural strengths of the mixes 50C35GGBS15CS and 80C10GGBS10CS were 10.27 MPa and 12.18 MPa, respectively. After 90 curing days, their flexural strengths were 13.17 MPa and 12.21 MPa, respectively. Similar results were reported by Laoufi et al. [2].

3.7. Mercury Intrusion Porosity (MIP)

The durability of mixes is related to their permeability. Moreover, the strength properties and freeze-thaw resistance strongly depend on their porous system [4,31]. Table 10 shows that the porosity has decreased with the curing time. The mix porosities were between 12% and 14%; 11% and 13%; 9% and 10%, and 7% and 11% after 7, 28, 56 and 90 curing days, respectively. Berodier and Scrivener (2015) [45] also reported that porosity could reach a long-term value equal to or lower than that of the cement mortar (control mix).

Table 10. Mix total porosities.

Curing Days	100C0GGBS0CS	50C35GGBS15CS	80C10GGBS10CS
7 days	14.25%	14.84%	12.62%
28 days	13.62%	12.43%	10.88%
56 days	9.85%	10.89%	10.74%
90 days	6.91%	11.02%	10.10%

Figure 13 shows the pore size distributions at 28, 56, and 90 curing days for the different mixes. The curve peaks represent the critical pore sizes. The replacement of cement by supplementary materials led to a porosity decrease and a mechanical strength increase. The graphs below show the effect of substitution of cement by the supplementary materials on the pore structure. A mix with 10% of GGBS and CS showed a critical pore size (0.095 µm) close to that of the control mortar (0.125 µm) after 28 days of curing. After 56 days of curing, the pore sizes became finer for all mixes. The pore size distribution in the mixes containing GGBS and CS was qualitatively different from that of the control. The pore size distribution peaks could be attributed to the cement hydrates which formed at the early age. On the other hand, the large range of pores (left of the curve) seems to be the result of GGBS and CS reactions, which become more pronounced with curing age [46].

Berodier and Scrivener (2015) [45] reported that the refinement of the pore structures by the production of hydrates inside the pores was due to the pozzolanic activity in the mixes containing supplementary materials.

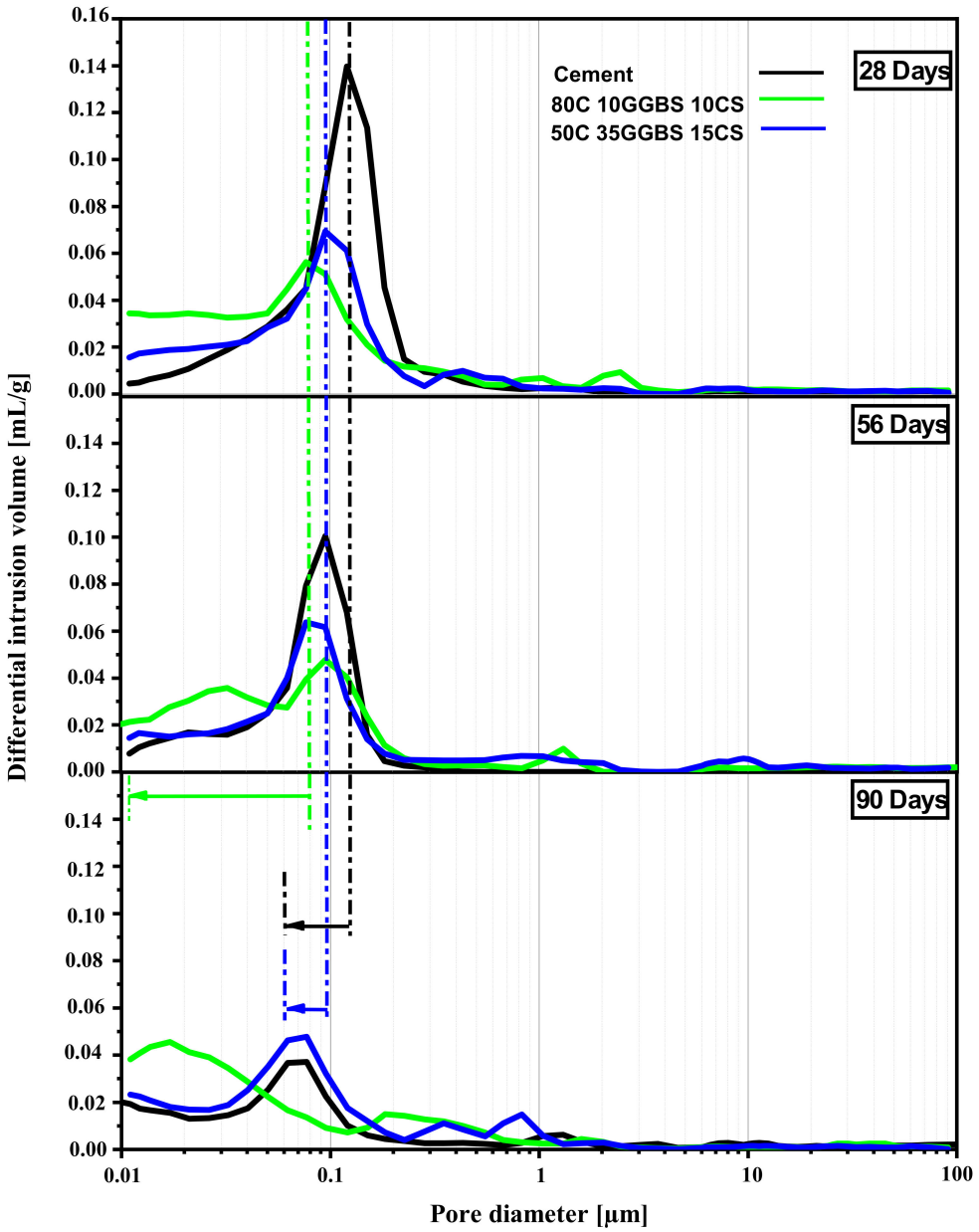

Figure 13. Mix pore size structures after 28, 56, and 90 days of curing.

The classification of porosity according to the diameter of the pores makes it possible to distinguish four types of porosity: harmless porosity (<20 nm), less harmful porosity (20–50 nm), harmful porosity (20–50 nm), and more harmful porosity (>200 nm) [46]. This classification is an indication of the durability of the mix. Figure 14 shows an increase in the harmful porosities for the control mix with the curing age, compared to those containing GGBS and CS. Moreover, there is an increase in harmless porosity for mixes containing GGBS and CS, which can be attributed to the effect of their pozzolanic activities. These results correlate well with those related to mechanical performances.

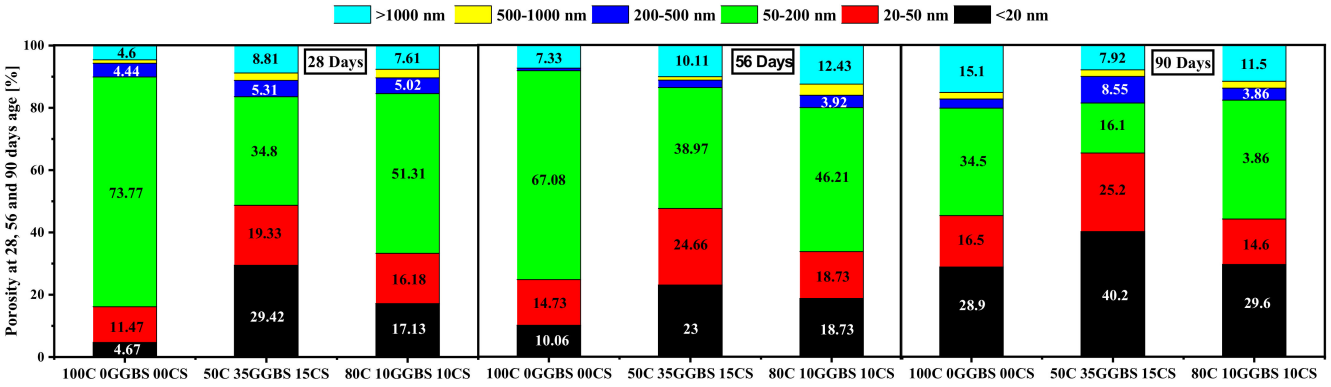

Figure 14. Distribution of porosities.

3.8. TG Quantification of Calcium Hydroxides

The thermogravimetric analysis was used to determine the quantity of portlandite consumed by the cement matrix of all mixes throughout the hydration process. The mixes were first dried until mass stabilization. Then, their particle granularities were decreased to a fine fraction using RS 200 vibratory Disc Mill by Retsch. The decomposition of portlandite ($Ca(OH)_2$) occurs between the temperatures of 4000C and 550 °C [39]. Table 11 and Figure 15 show a significant decrease (more than 50%) in the portlandite content for the mixes 80C10GGBS10CS and 50C35GGBS15CS. After 7 days of curing, the portlandite rates were 10.50% and 13.91% for 50C35GGBS15CS and 80C10GGBS10CS, respectively. However, they decreased to 2.88% and 0.82% after 90 days of curing. The decrease in calcium hydroxide for both mixes may be linked to the pozzolanic character of GGBS and CS aluminosilicates, which react with $Ca(OH)_2$ formed during cement hydration. These pozzolanic reactions generate additional C-S-H, which contribute to improving the mechanical performance of the mixes. However, the control mix portlandite content, which remained relatively constant for the different curing times, was equal to 6.54%, 6.96%, 6.54% and 5,52% after 7, 28, 56, and 90 days of curing, respectively. The consumption of portlandite in blended cement by supplementary materials is a good indication of the pozzolanic potential of the used materials [39]. Several previous studies have reported similar behaviors [39,47,48].

Table 11. Portlandite percent content after 7, 28, 56, and 90 days of curing.

Curing Days	100C0GGBS0CS	50C35GGBS15CS	80C10GGBS10CS
7 days	6.54%	10.50%	13.91%
28 days	6.96%	3.62%	5.43%
56 days	6.54%	4.07%	5.97%
90 days	5.52%	5.97%	0.82%

3.9. Scanning Electron Microscopy (SEM)

Figures 16–18 show the microstructure of hydrated control and 50C35GGBS15CS mixes at 56 curing days. Figures 16 and 17 show the Inner C-S-H, which is a thin light grey (uniform) layer that surrounds the unreacted cement grains. The heterogeneous outer C-S-H includes grey and black areas (porous area). It consists of pores, precipitated C-S-H, ettringite (AFt), and monosulfate (AFm) located between the grains to replace water filled-space [49]. The portlandite (CH) is shown in a grey that is slightly lighter than that of the Inner C-S-H.

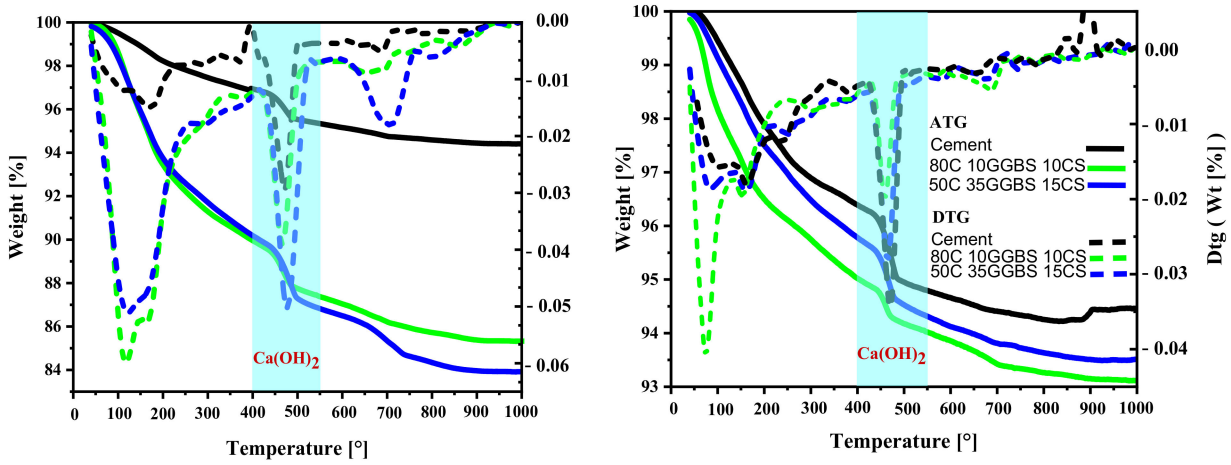

(**a**) (**b**)

Figure 15. Thermogravimetric analysis after (**a**) 7 and (**b**) 56 curing days of all mixes.

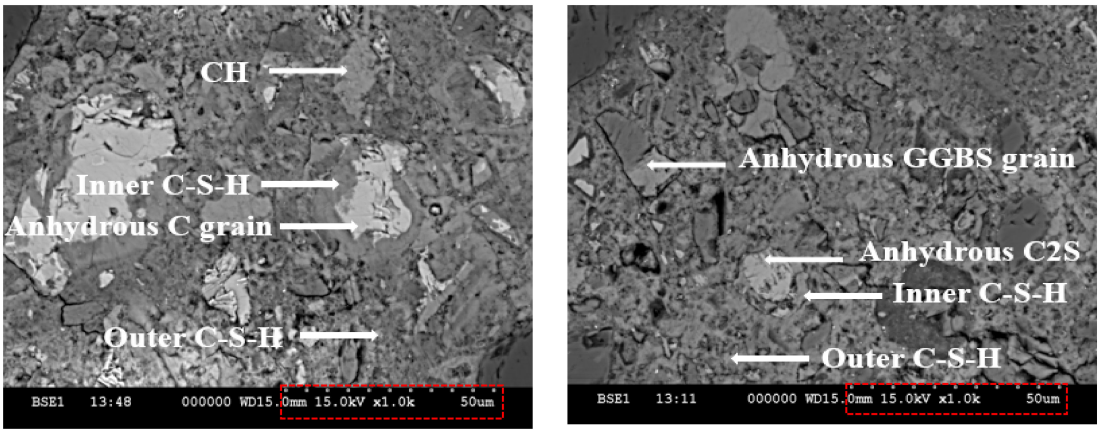

(**a**) (**b**)

Figure 16. SEM observations after 56 curing days of (**a**) control mix and (**b**) mix 50C35GGBS15CS.

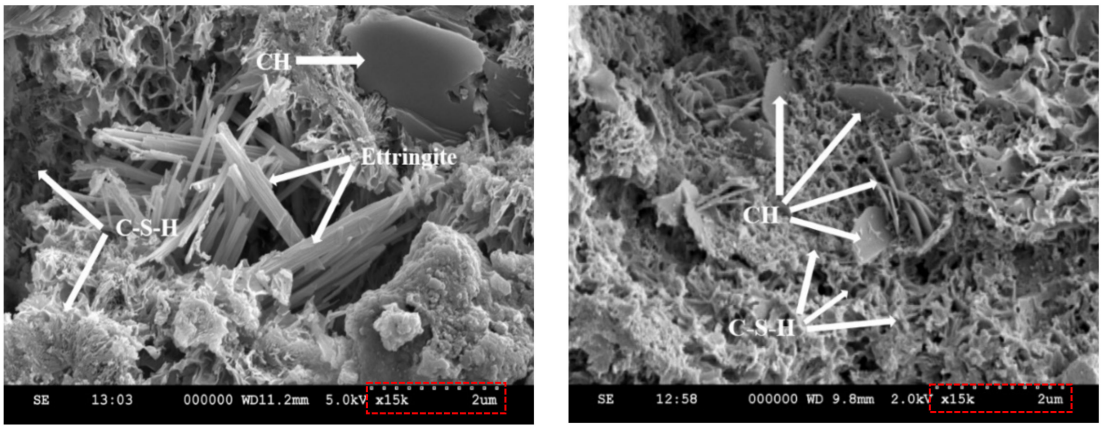

(**a**) (**b**)

Figure 17. SEM observations after 56 curing days of (**a**) control mix and (**b**) mix 50C35GGBS15CS.

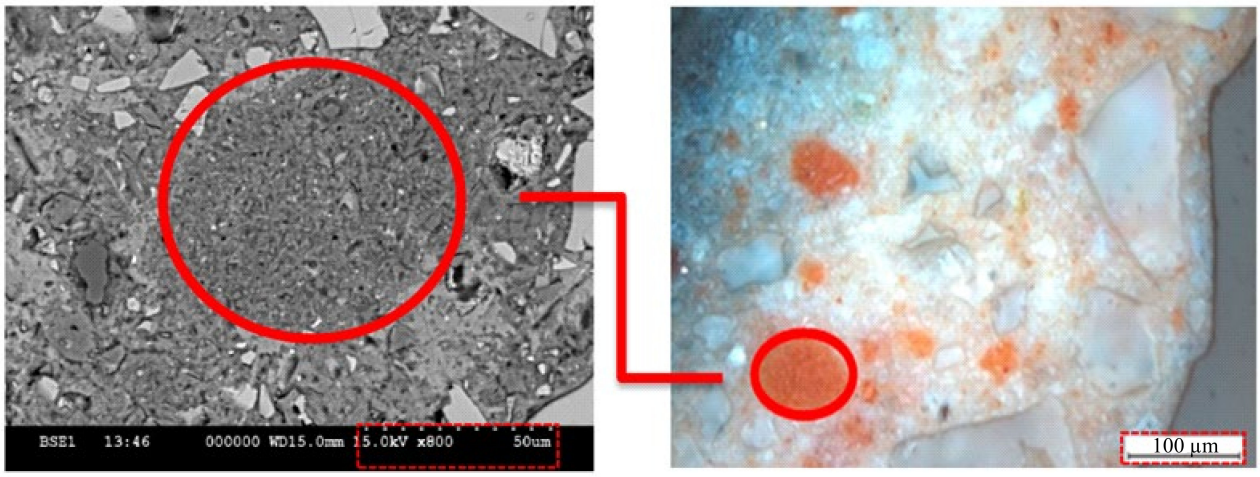

Figure 18. SEM (**a**) and optical (**b**) microscopy on 80C10GGBS10CS after 56 days of curing.

Figure 16b, Figure 17b, and Figure 18b show denser and more consistent Outer C-S-H areas than those in Figures 16a, 17a and 18a. This is due to the process of hydration, which continues to produce new hydrates filling the voids between the grains [29,50,51], especially for the mixes 50C35GGBS15CS and 80C10GGBS10CS because of the pozzolanic reactions.

3.10. Mix Leaching Tests

The environmental impact was assessed by analyzing the trace elements that can leach to water sources. The durability of concretes and mortars is influenced by certain parameters and their combination, and knowledge of these is essential in order to extend their life cycle [52]. A leaching test was carried out on the mixes 100C00GGBS00CS, 50C35GGBS15CS, and 80C10GGBS after 56 curing days according to NF EN 12457-2. It was carried out on eluates filtered at 0.45 µm, which were obtained from leaching of crushed mortars with a particle size distribution between 0 and 4 mm in ultra-pure water for 24 h, with a liquid/solid ratio of 10. Table 12 summarizes the concentrations of trace elements present in the eluates of the mixes. The concentrations of the heavy metals remain below the detection thresholds of measuring devices and lower than that of the raw sediments. Moreover, the anion concentrations (chloride, fluoride, and sulfate) remain below the threshold limits for inert waste. However, the sulfate concentrations in the control mix (22 mg/kg DM) are higher than those in the mixes based on GGBS and CS. This can be explained by the substitution of cement by GGBS and CS and by the participation of sulfates in the formation of new ettringite. Adu-Amankwah et al. (2018) [53] reported that when they reach a certain concentration, the sulfates in ternary binders increase the volume of ettringite formation and improve mechanical behavior of the mixtures.

All mixes qualify as inert wastes because their element concentrations in the eluate are lower than the threshold limits that were established by the French directive concerning storage facilities (French Directive of 14 December 2014).

Table 12. Eluate element concentrations compared to inert waste leching limit values (French Directive of 14 December 2014).

Elements	100C0GGBS00CS	50C35GGBS15CS	80C10GGBS10CS	IWR (mg/kg of Dry Matter)
As	<0.110	<0.110	<0.110	0.500
Cd	<0.009	<0.009	<0.009	0.040
Cr	0.031	<0.004	<0.004	0.500
Cu	<0.021	<0.021	<0.021	2.000
MO	<0.088	<0.088	<0.088	0.500
Ni	<0.047	<0.047	<0.047	0.400
Pb	<0.032	<0.032	<0.032	0.500
Sb	<0.057	<0.057	<0.057	0.060
Se	<0.083	<0.083	<0.083	0.100
Zn	<0.010	<0.010	<0.010	4.000
Chloride	43	42	45	800
Fluoride	4	4	3	10
Sulfate	22	13	13	1000

4. Conclusions

This study investigated the potential use of Zerdezas dam Calcined Sediments (CS) and El- Hadjar Blast Furnace Slag (GGBS) from northern Algeria as a partial replacement of cement (C) in normal hardening hydraulic road binders. Two binder mixture designs were optimized using a Response Surface Methodology (RSM). The first mix, 50C35GGBS15CS, consisted of 50% cement, 35% blast furnace slag, and 15% calcined sediment. The second mix, 80C10GGBS10CS, consisted of 80% cement, 10% blast furnace slag, and 10% calcined sediments. Both binders satisfied all the requirements for hydraulic binders specified in the EN 13282-2 standard. The tests of workability, setting time, volume expansion, compressive and flexural strengths, porosity, and SEM were conducted to ensure that both mixes meet the requirements for road construction binders. The following conclusions can be drawn:

1. Both mixtures are qualified as plastic mixes because their flow values were higher than the threshold limit of 140 mm (RS, 2015). The cement substitution by supplementary materials led to a negligible decrease in workability compared to the control mix.
2. The setting times of the formulated hydraulic road binders are suitable because they are greater than the limit value of 150 min.
3. The sulfate contents for both mixes containing GGBS and Calcined sediments were well below than 4%, which is required value for hydraulic road binders with normal hardening according EN 13282-2 standard.
4. The volume expansions were higher than that of the control (0.33 mm). However, the increased volume expansions remain very low and not significant when compared to the threshold limit value of 30 mm for normal hardening hydraulic road binders (EN 13282-2).
5. At 56 days of curing, the compressive strength values ranging between 32.5 MPa and 52.5 MPa, met the mechanical strength requirements for normal hardening hydraulic road binders (class N4) according to EN 13282-2.
6. The replacement of cement by supplementary materials led to a porosity decrease, refined porosity distribution, and mechanical strength increase.
7. The incorporation of GGBS and calcined sediments on the mixt exhibited an increase in harmless porosity.
8. The concentrations of heavy metals on the mix containing GGBS and calcined sediments remained below the detection thresholds of measuring devices and lower than that of the raw sediments. Moreover, their anion concentrations (chloride, fluoride, and sulfate) remained below the threshold limits for Inert Waste (French Directive of 14 December 2014).

The two proposed hydraulic road binders are qualified as normal hardening hydraulic road binders with the following designations (EN 13282-2): HRB N 4–C 50, GGBS 35, CS 15

for mix 50C35GGBS15CS, and HRB N 4–C 80, GGBS 10, CS 10 for mix 80C10GGBS10CS. Therefore, their use in road construction will be addressed in future studies.

The reuse of the GGBS and calcined sediments will contribute to a better disposal of dam sediments and steel industry waste. It will also contribute to the environmental impact reduction of clinker production by reducing greenhouse gas emissions.

Author Contributions: Conceptualization, S.B.; Data curation, S.B.; Formal analysis, W.M.; Investigation, S.B. and W.M.; Methodology, S.B., W.M. and S.M.; Project administration, M.H.; Resources, W.M.; Supervision, W.M. and S.M.; Validation, S.B.; Writing—original draft, S.B.; Writing—review & editing, W.M., S.M. and A.S. All authors have read and agreed to the published version of the manuscript.

Funding: This research received no external funding.

Institutional Review Board Statement: Not applicable.

Informed Consent Statement: Not applicable.

Data Availability Statement: The data presented in this study are available on request from the corresponding author.

Acknowledgments: This work was conducted in the laboratory of the Centre of materials and Process of IMT Lille Douai. The authors would like to thank the team of the Civil and Environmental Engineering laboratory at the IMT for their support and cooperation over this period. Our sincere thanks also go to the Vincent Thiery for the optical microscope image.

Conflicts of Interest: The authors declare no conflict of interest.

References

1. Scrivener, K.L.; John, V.M.; Gartner, E.M. Eco-Efficient Cements: Potential Economically Viable Solutions for a Low-CO_2 Cement-Based Materials Industry. *Cem. Concr. Res.* **2018**, *114*, 2–26. [CrossRef]
2. Laoufi, L.; Senhadji, Y.; Benazzouk, A. Valorization of Mud from Fergoug Dam in Manufacturing Mortars. *Case Stud. Constr. Mater.* **2016**, *5*, 26–38. [CrossRef]
3. Rivera, R.A.; Sanjuán, M.Á.; Martín, D.A. Granulated Blast-Furnace Slag and Coal Fly Ash Ternary Portland Cements Optimization. *Sustainability* **2020**, *12*, 5783. [CrossRef]
4. Benzerzour, M.; Maherzi, W.; Amar, M.A.A.; Abriak, N.E.; Damidot, D. Formulation of Mortars Based on Thermally Treated Sediments. *J. Mater. Cycles Waste Manag.* **2018**, *20*, 592–603. [CrossRef]
5. Segui, P.; Aubert, J.E.; Husson, B.; Measson, M. Utilization of a Natural Pozzolan as the Main Component of Hydraulic Road Binder. *Constr. Build. Mater.* **2013**, *40*, 217–223. [CrossRef]
6. Yu, J.; Wu, H.L.; Mishra, D.K.; Li, G.; Leung, C.K. Compressive Strength and Environmental Impact of Sustainable Blended Cement with High-Dosage Limestone and Calcined Clay (LC2). *J. Clean. Prod.* **2021**, *278*, 123616. [CrossRef]
7. Hameed, R.; Seo, J.; Park, S.; Amr, I.T.; Lee, H.K. CO_2 Uptake and Physicochemical Properties of Carbonation-Cured Ternary Blend Portland Cement–Metakaolin–Limestone Pastes. *Materials* **2020**, *13*, 4656. [CrossRef] [PubMed]
8. Juenger, M.C.G.; Snellings, R.; Bernal, S.A. Supplementary Cementitious Materials: New Sources, Characterization, and Performance Insights. *Cem. Concr. Res.* **2019**, *122*, 257–273. [CrossRef]
9. *IEA-CSI Technology Roadmap for Cement*; International Energy Agency: Paris, France, 2018.
10. Pade, C.; Guimaraes, M. The CO_2 Uptake of Concrete in a 100 Year Perspective. *Cem. Concr. Res.* **2007**, *37*, 1348–1356. [CrossRef]
11. Li, J.; Tharakan, P.; Macdonald, D.; Liang, X. Technological, Economic and Financial Prospects of Carbon Dioxide Capture in the Cement Industry. *Energy Policy* **2013**, *61*, 1377–1387. [CrossRef]
12. Shanks, W.; Dunant, C.F.; Drewniok, M.P.; Lupton, R.C.; Serrenho, A.; Allwood, J.M. How Much Cement Can We Do without? Lessons from Cement Material Flows in the UK. *Resour. Conserv. Recycl.* **2019**, *141*, 441–454. [CrossRef]
13. Dixit, A.; Du, H.; Pang, S.D. Carbon Capture in Ultra-High Performance Concrete Using Pressurized CO_2 Curing. *Constr. Build. Mater.* **2021**, *288*, 123076. [CrossRef]
14. Scrivener, K.; Martirena, F.; Bishnoi, S.; Maity, S. Calcined Clay Limestone Cements (LC3). *Cem. Concr. Res.* **2018**, *114*, 49–56. [CrossRef]
15. Men, G.; Bonavetti, V.; Irassar, E.F. Strength Development of Ternary Blended Cement with Limestone Filler and Blast-Furnace Slag. *Cem. Concr. Compos.* **2003**, *25*, 61–67.
16. Bágel, L. Strength and pore structure of ternary blended cement mortars containing blast furnace slag and silica fume. *Cem. Concr. Res.* **1998**, *28*, 1011–1020. [CrossRef]
17. Shanmuga Priya, D.; Sakthieswaran, N.; Ganesh Babu, O. Experimental Study on Mortar as Partial Replacement Using Sawdust Powder and GGBS 2020. *Mater. Today Proc.* **2021**, *37*, 1051–1055. [CrossRef]

18. Toumi, A.; Remini, B. Zardezas (algeria): A dam that is silting up? zardezas (algerie): UN barrage qui s'envase? *LARHYSS J.* **2020**, *43*, 7–22.
19. Benzerzour, M.; Amar, M.; Abriak, N.E. New Experimental Approach of the Reuse of Dredged Sediments in a Cement Matrix by Physical and Heat Treatment. *Constr. Build. Mater.* **2017**, *140*, 432–444. [CrossRef]
20. Dang, T.A.; Kamali-Bernard, S.; Prince, W.A. Design of New Blended Cement Based on Marine Dredged Sediment. *Constr. Build. Mater.* **2013**, *41*, 602–611. [CrossRef]
21. Hadj Sadok, R.; Belas, N.; Tahlaiti, M.; Mazouzi, R. Production, Reusing Calcined Sediments from Chorfa II Dam as Partial Replacement of Cement for Sustainable Mortar. *J. Build. Eng.* **2021**, *40*, 102273. [CrossRef]
22. Snellings, R.; Cizer, Ö.; Horckmans, L.; Durdziński, P.T.; Dierckx, P.; Nielsen, P.; van Balen, K.; Vandewalle, L. Properties and Pozzolanic Reactivity of Flash Calcined Dredging Sediments. *Appl. Clay Sci.* **2016**, *129*, 35–39. [CrossRef]
23. van Bunderen, C.; Snellings, R.; Vandewalle, L.; Cizer, Ö. Early-Age Hydration and Autogenous Deformation of Cement Paste Containing Flash Calcined Dredging Sediments. *Constr. Build. Mater.* **2019**, *200*, 104–115. [CrossRef]
24. van Bunderen, C.; Benboudjema, F.; Snellings, R.; Vandewalle, L.; Cizer, Ö. Experimental Analysis and Modelling of Mechanical Properties and Shrinkage of Concrete Recycling Flash Calcined Dredging Sediments. *Cem. Concr. Compos.* **2021**, *115*, 103787. [CrossRef]
25. Stevulova, N.; Strigáč, J.; Junak, J.; Terpakova, E.; Holub, M. Incorporation of Cement Bypass Dust in Hydraulic Road Binder. *Materials* **2021**, *14*, 41. [CrossRef]
26. Behim, M.; Cyr, M.; Clastres, P. Physical and Chemical Effects of El Hadjar Slag Used as an Additive in Cement-Based Materials. *Eur. J. Environ. Civ. Eng.* **2011**, *15*, 1413–1432. [CrossRef]
27. Remini, B.; Hallouche, W.; Achour, B. L'algerie: Plus D'un Siecle 2 De Desenvasement Des 3 Barrages. 2020. Available online: https://www.researchgate.net/publication/343636574_PARTIE_II_-LES_EAUX_DOUCES_ET_DE_SURFACE_CHAPITRE_8_L\T1\textquoterightALGERIE_PLUS_D\T1\textquoterightUN_SIECLE_2_DE_DESENVASEMENT_DES (accessed on 23 September 2021).
28. Alujas, A.; Fernández, R.; Quintana, R.; Scrivener, K.L.; Martirena, F. Pozzolanic Reactivity of Low Grade Kaolinitic Clays: Influence of Calcination Temperature and Impact of Calcination Products on OPC Hydration. *Appl. Clay Sci.* **2015**, *108*, 94–101. [CrossRef]
29. Sadok, R.H.; Maherzi, W.; Benzerzour, M.; Lord, R.; Torrance, K.; Zambon, A.; Abriak, N. Mechanical Properties and Microstructure of Low Carbon Binders Manufactured from Calcined Canal Sediments and Ground Granulated Blast Furnace Slag (GGBS). *Sustainability* **2021**, *13*, 9057. [CrossRef]
30. Nozahic, V. Vers Une Nouvelle Démarche de Conception Des Bétons de Végétaux Lignocellulosiques Basée Sur La Compréhension et L'amélioration de L'interface Liant/Végétal: Application à Des Granulats de Chenevotte et de Tige de Tournesol Associés à Un Liant Ponce/chaux. Ph.D Thesis, Université Blaise Pascal, Clermont-Ferrand, France, 2012.
31. Bouchikhi, A.; Maherzi, W.; Benzerzour, M.; Mamindy-Pajany, Y.; Peys, A.; Abriak, N.E. Manufacturing of Low-Carbon Binders Using Waste Glass and Dredged Sediments: Formulation and Performance Assessment at Laboratory Scale. *Sustainability* **2021**, *13*, 4960. [CrossRef]
32. Avet, F.; Snellings, R.; Alujas Diaz, A.; ben Haha, M.; Scrivener, K. Development of a New Rapid, Relevant and Reliable (R3) Test Method to Evaluate the Pozzolanic Reactivity of Calcined Kaolinitic Clays. *Cem. Concr. Res.* **2016**, *85*, 1–11. [CrossRef]
33. Herrero, A.; Ortiz, M.C.; Sarabia, L.A. D-Optimal Experimental Design Coupled with Parallel Factor Analysis 2 Decomposition a Useful Tool in the Determination of Triazines in Oranges by Programmed Temperature Vaporization-Gas Chromatography-Mass Spectrometry When Using Dispersive-Solid Phase Ex. *J. Chromatogr. A* **2013**, *1288*, 111–126. [CrossRef] [PubMed]
34. Fatemi, S.; Varkani, M.K.; Ranjbar, Z.; Bastani, S. Optimization of the Water-Based Road-Marking Paint by Experimental Design, Mixture Method. *Prog. Org. Coat.* **2006**, *55*, 337–344. [CrossRef]
35. Li, X.; Huang, H.; Xu, J.; Ma, S.; Shen, X. Statistical Research on Phase Formation and Modification of Alite Polymorphs in Cement Clinker with SO_3 and MgO. *Constr. Build. Mater.* **2012**, *37*, 548–555. [CrossRef]
36. Imanzadeh, S.; Hibouche, A.; Jarno, A.; Taibi, S. Formulating and Optimizing the Compressive Strength of a Raw Earth Concrete by Mixture Design. *Constr. Build. Mater.* **2018**, *163*, 149–159. [CrossRef]
37. Zeraoui, A. Approche Opérationnelle Pour Une Gestion Durable des Sédiments de Dragage dans des Filières de Génie Civil: Mise en Place d'un Outil D'aide à la Décision. Ph.D Thesis, Université de Lille, Douai, France, 2020.
38. el Mahdi Safhi, A.; Benzerzour, M.; Rivard, P.; Abriak, N.E. Feasibility of Using Marine Sediments in SCC Pastes as Supplementary Cementitious Materials. *Powder Technol.* **2019**, *344*, 730–740. [CrossRef]
39. Fernandez, R.; Scrivener, K. Calcined Clayey Soils as a Potential Replacement for Cement in Developing Countries. Ph.D Thesis, Ecole Polytechnique Fédérale de Lausanne, Lausanne, Switzerland, 2009; p. 178.
40. Bouchikhi, A.; Benzerzour, M.; Abriak, N.E.; Maherzi, W.; Mamindy-Pajany, Y. Study of the Impact of Waste Glasses Types on Pozzolanic Activity of Cementitious Matrix. *Constr. Build. Mater.* **2019**, *197*, 626–640. [CrossRef]
41. Mobili, A.; Belli, A.; Giosuè, C.; Bellezze, T.; Tittarelli, F. Metakaolin and Fly Ash Alkali-Activated Mortars Compared with Cementitious Mortars at the Same Strength Class. *Cem. Concr. Res.* **2016**, *88*, 198–210. [CrossRef]
42. Samet, B.; Mnif, T.; Chaabouni, M. Use of a Kaolinitic Clay as a Pozzolanic Material for Cements: Formulation of Blended Cement. *Cem. Concr. Compos.* **2007**, *29*, 741–749. [CrossRef]

43. Wang, L.; Ur, N.; Curosu, I.; Zhu, Z.; Abdul, M.; Beigh, B.; Liebscher, M.; Chen, L.; Tsang, D.C.W.; Hempel, S.; et al. Cement and Concrete Research On the Use of Limestone Calcined Clay Cement (LC3) in High-Strength Strain-Hardening Cement-Based Composites (HS-SHCC). *Cem. Concr. Res.* **2021**, *144*, 106421. [CrossRef]
44. Kuri, J.C.; Khan, M.N.N.; Sarker, P.K. Fresh and Hardened Properties of Geopolymer Binder Using Ground High Magnesium Ferronickel Slag with Fly Ash. *Constr. Build. Mater.* **2021**, *272*, 121877. [CrossRef]
45. Berodier, E.; Scrivener, K. Evolution of Pore Structure in Blended Systems. *Cem. Concr. Res.* **2015**, *73*, 25–35. [CrossRef]
46. Zhao, S.; Xia, M.; Yu, L.; Huang, X.; Jiao, B.; Li, D. Optimization for the Preparation of Composite Geopolymer Using Response Surface Methodology and Its Application in Lead-Zinc Tailings Solidification. *Constr. Build. Mater.* **2021**, *266*, 120969. [CrossRef]
47. Briki, Y.; Avet, F.; Zajac, M.; Bowen, P.; Haha, M.B.; Scrivener, K. Understanding of the Factors Slowing down Metakaolin Reaction in Limestone Calcined Clay Cement (LC3) at Late Ages. *Cem. Concr. Res.* **2021**, *146*, 106477. [CrossRef]
48. Zhou, Y.F.; Li, J.S.; Lu, J.X.; Cheeseman, C.; Poon, C.S. Sewage Sludge Ash: A Comparative Evaluation with Fly Ash for Potential Use as Lime-Pozzolan Binders. *Constr. Build. Mater.* **2020**, *242*, 118160. [CrossRef]
49. Scrivener, K.L. Backscattered Electron Imaging of Cementitious Microstructures: Understanding and Quantification. *Cem. Concr. Compos.* **2004**, *26*, 935–945. [CrossRef]
50. Hadj-Sadok, A.; Kenai, S.; Courard, L.; Darimont, A. Microstructure and Durability of Mortars Modified with Medium Active Blast Furnace Slag. *Constr. Build. Mater.* **2011**, *25*, 1018–1025. [CrossRef]
51. Ahmed, H. sadok Effect of the Microstructure of Mortars with Low Hydraulicity Slag on Their Behavior in Aggressive Environments. *MATEC Web Conf.* **2018**, *149*, 01025. [CrossRef]
52. Lehner, P.; Ghosh, P.; Konečný, P. Statistical Analysis of Time Dependent Variation of Diffusion Coefficient for Various Binary and Ternary Based Concrete Mixtures. *Constr. Build. Mater.* **2018**, *183*, 75–87. [CrossRef]
53. Adu-Amankwah, S.; Black, L.; Skocek, J.; ben Haha, M.; Zajac, M. Effect of Sulfate Additions on Hydration and Performance of Ternary Slag-Limestone Composite Cements. *Constr. Build. Mater.* **2018**, *164*, 451–462. [CrossRef]